Asian Journal of Chemistry; Vol. 30, No. 8 (2018), 1736-1742

ASIAN JOURNAL OF CHEMISTRY

https://doi.org/10.14233/ajchem.2018.21310

Thermally Stable and Processable Organic-Inorganic Hybrid Material

GEETHY P. GOPALAN and RAJU FRANCIS*

School of Chemical Sciences, Mahatma Gandhi University, Kottayam-686 560, India

*Corresponding author: Tel: +91 481 2731036; E-mail: rajufrancis@mgu.ac.in

Received: 1 March 2018; *Accepted*: 24 April 2018; *Published online*: 30 June 2018; AJC-18965

This article presents a simple and facile method to produce thermoresponsive organic-inorganic hybrid materials. They are prepared by fine-tuning the synthetic protocol for coupling N-isopropyl acrylamide, maleic anhydride and aminopropyl triethoxy silane through sol-gel technique in the absence of externally added acid or base catalyst. The spectroscopic and microscopic characterization follows standard procedures. The formation of highly porous inorganic nanodomains as a function of feed ratio is explained with the support of microscopic studies. The thermal stability and crystallinity studies are also done to propose for drug delivery or specific insulator applications. The dielectric property of this hybrid material is compared with similar materials for commercial applications.

Keywords: Sol-gel, Thermoresponsive, N-isopropylacrylamide, Hybrid materials.

INTRODUCTION

Organic-inorganic hybrid materials can be made up of organic-inorganic components called nanocomposites; its length changed from angstroms to nanometers. These materials can be prepared by the development of soft inorganic chemistry process mainly sol-gel process [1]. They are very much attractive in many areas such as optical, electrical, ionic sensors, biosensors, catalysts, *etc*. They were mainly based on metal alkoxide systems particularly organosilanes and also merge with organic molecules, polymers and biocomponents. Especially aminopropyl functionalized silanes have vast interest and also have huge consideration.

These materials achieve outstanding properties such as mechanical properties, thermal stability, degradation and abrasion resistance [2-5]. As a result, these polymer-inorganic hybrid materials have a lot of importance in the recent research. There are different ways to synthesize these materials. They are sol-gel method, surface-initiated ATRP and free radical polymerization [6-8]. There is an efficient technique to develop the interface compatibility and miscibility of the organic-inorganic materials with the polymeric matrix. For this silica nanoparticles are modified with the coupling agents, in order to increase the characteristics of the composite materials [9].

One of the most studied and well-known temperature-responsive polymers is poly N-isopropyl acrylamide (PNIPAM), its LCST is 32 ºC which is near to our body temperature [10,11]. Temperature responsive polymers exhibit a sudden change in their physico-chemical properties due to temperature variation so that they are extensively studied nowadays in different fields. There are a lot of materials can be prepared from thin films such as layer by layer hybrid film and brushes, membranes, colloids, micelles, nanogels, *etc*. [12].

Silica is used as the inorganic component for the synthesis of organic-inorganic composites and it possesses high thermal and mechanical stability. It is an outstanding insulator and also it acquires high band gap and dielectric strength [13,14]. The high dielectric constant can be achieved by the incorporation of different fillers such as SiO_2, $BaSrTiO_3$, $BaTiO_3$, graphene and multi-wall carbon nanotubes (MWCNTs) and they were reported in several studies [15,16]. However, the processability of bare silica for specific applications is a limitation.

Several methods were reported on the synthesis of PNIPAM /SiO_2 hybrid materials [17,18]. Some researchers developed these materials using surface-initiated ATRP. The obtained materials were core shell-like structure and showed the good thermoresponsive property. It was suggested that they were applicable to the fields of biological and biomedical fields [19,20]. In another strategy, using sol-gel process was a sequence of numerous SiO_2 particles embedded with PNIPAM particles at room temperature [20]. Other approaches were grafting of silica onto PNIPAM particles using RAFT polymerization and radical polymerization. These grafted materials have several applications in various fields [21-23].

The synthesis of poly(N-isopropylacrylamide-*co*-maleic anhydride) (NIPAM-*co*-MA) was reported earlier, by using free radical polymerization reaction [24,25]. Poly(styrene-*co*-maleic anhydride)/silica hybrid material has been successfully prepared

from styrene-maleic anhydride copolymer and tetraethoxysilane (TEOS) in the presence of a coupling agent, APTES by an *in situ* sol-gel process [26]. However, there are no reports on chemical linking of size-tunable silica nanoparticles onto NIPAM polymer through maleic anhydride coupling reaction. Additionally, the possibility of avoiding the addition of any external catalyst during the sol-gel process is also attempted in this work.

In this regard, the current study is focused on the synthesis of hybrid materials by fine-tuning the synthetic protocol for coupling N-isopropyl acrylamide, maleic anhydride and aminopropyl triethoxy silane through sol-gel technique in the absence of externally added acid or base catalyst. The spectroscopic and microscopic characterization follows standard procedures. The formation of highly porous inorganic nanodomains as a function of feed ratio is explained with the support of microscopic data. The thermal stability and crystallinity studies are also done to propose for drug delivery or specific insulator applications. The dielectric property of this hybrid material is compared with similar materials for commercial applications.

EXPERIMENTAL

N-Isopropyl acrylamide (NIPAM), maleic anhydride (MA), α,α′-azobisisobutyronitrile (AIBN) (Sigma Aldrich), tetraethylorthosilicate (TEOS) (Merck), 3-aminopropyl triethoxy silane (APTES) (Spectrochem Ltd) were used as received. Maleic anhydride was purified from recrystallization using ethyl acetate. Solvents used were 1,4-dioxane and diethyl ether (Spectrochem Ltd). All solvents were purified according to Vogel's textbook (Organic Chemistry).

Synthesis of copolymer, N-isopropyl acrylamide-*co*-maleic anhydride copolymer 90:10 [24]**:** Copolymerization of NIPAM (1.102 g, 0.009 mol) with MA (0.098 g, 0.001 mol) was carried out using AIBN (0.082 g, 0.0005 mol) as thermal initiator was mixed thoroughly with sufficient amount of 1, 4-dioxane (2 mL) (**Scheme-I**). Nitrogen gas was purged for 20 min. The solution was placed at 70 ºC in an oil bath and kept for stirring. The viscous solution was poured into diethyl ether, and filtration recovered the precipitated polymer. Re-precipitating further purified the polymer from dioxane-ether system. Different monomer feed ratios 80:20, 70:30, 60:40, were also carried out using this same protocol.

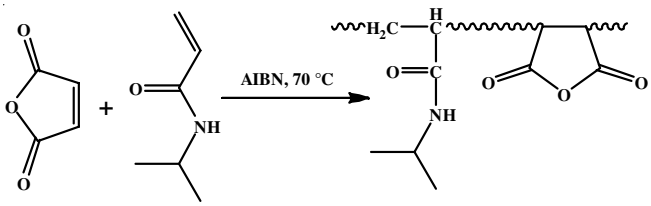

Scheme-I: Synthesis of NIPAM-*co*-MA

Synthesis of hybrid material (NIPAM-*co*-MA)/SiO_2: NIPAM-*co*-MA with various monomer feed ratios were applied for the synthesis of hybrid materials. The copolymer (1 g) was mixed with THF. APTES (0.23 mL) and TEOS (0.22 mL) were mixed and agitated in a sonicator for one minute. The polymer solution was added to this solution and stirred to get a viscous solution (**Scheme-II**). The obtained viscous solution was dried at room temperature and then cured at 60 ºC under vacuum for one day to expel any residual alcohol or solvent. The obtained hybrid material was purified by washing with THF and dried.

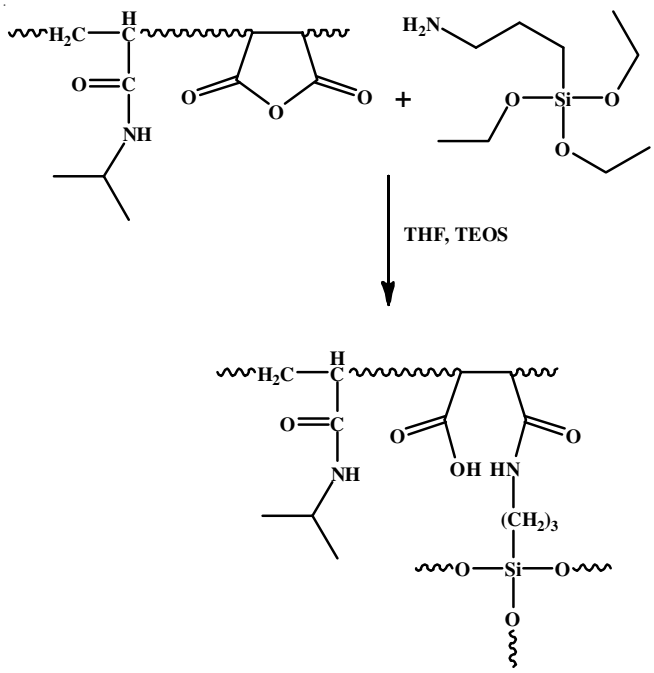

Scheme-II: Synthesis of (NIPAM-*co*-MA)/SiO_2

Fourier Transform Infrared Spectroscopy (FTIR) spectra were recorded on a Bruker instrument (Alpha T) at room temperature. The prepared samples were mixed with KBr to obtain the FTIR spectra. The surface morphology of prepared hybrid materials was viewed with scanning electron microscopy (SEM) after thin coating with gold. Transmission electron microscopy (TEM) was performed on a JEOL JEM-2010 high-resolution transmission electron microscope at an acceleration voltage of 120 kV. Atomic force microscopy observations were carried out in the air on as received sample surfaces using WITec Alpha 300RA Confocal Raman microscope with AFM operated in non-contact tapping mode. The samples were coated on a glass slide and dried at room temperature. The thermal analysis was carried out using Pyris I TGA Thermo Gravimetric analyzer (Perkin Elmer) under a nitrogen atmosphere, at a heating rate of 10 ºC/min. Crystal studies were performed using an X'Pert Pro PANalytical X-ray powder diffractometer with Ni-filtered Cu Kα X-ray radiation. Dielectric studies were done by using Agilent precision LCR series meter with frequency 100Hz to 2MHz. Sample thickness was around 2 mm and diameter 1.2 cm.

RESULTS AND DISCUSSION

The chemically linked organic-inorganic hybrid material was synthesized by using stimuli-responsive NIPAM-*co*-MA copolymer with functionalized silane. An external acid catalyst is generally needed for the construction of silica network. In this (NIPAM-*co*-MA)/SiO_2 hybrid material, maleic anhydride is converted to maleamic acid. The ring opening took place, and the acid itself acted as a catalyst for the spontaneous development of silica network during the sol-gel process.

FTIR spectra of NIPAM-*co*-MA copolymer (Fig. 1A) with different monomer ratios were characterized. The characteristic absorption peaks were obtained in the regions 3200 cm^{-1} for the secondary NH amide groups, 2987-2973 cm^{-1} CH bands in isopropyl groups. The bands at 1844 and 1773 cm^{-1} correspond to the anhydride units in MA. A peak at 1695 cm^{-1} correspond to C=O stretching of amide I peak and NH bending peak at 1547cm^{-1}. The monomer ratios were increased up to 60:40, a new peak obtained in the region 1692 cm^{-1} which correspond to acid C=O peak. The reason is that some maleic anhydride units were changed to maleamic acid before the sol-gel process.

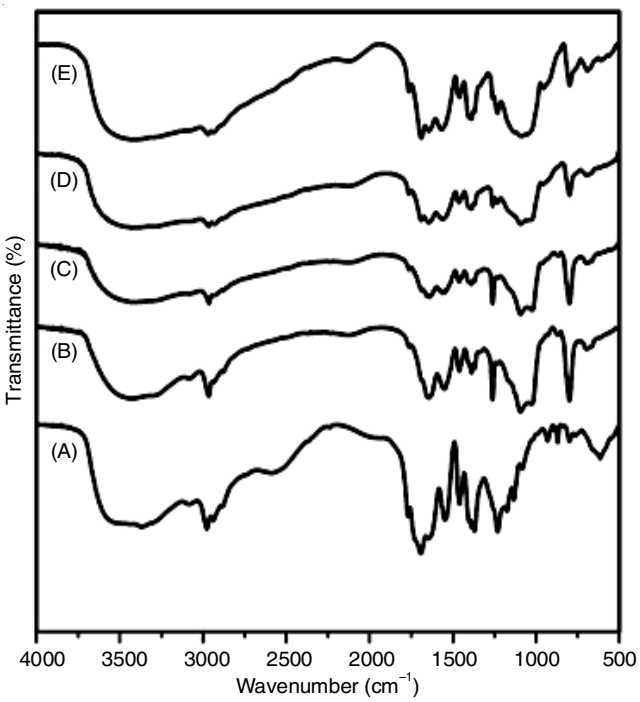

Fig. 1. FTIR traces of (A) $NIPAM_{60}$-*co*-MA_{40} and hybrid materials (B) ($NIPAM_{90}$-*co*-MA_{10})/SiO_2 (C) ($NIPAM_{80}$-*co*-MA_{20})/SiO_2 (D) ($NIPAM_{70}$-*co*-MA_{30})/SiO_2 (E) ($NIPAM_{60}$-*co*-MA_{40})/SiO_2

Fig. 1(B-E) represents the FT-IR spectra of ($NIPAM_{90}$-*co*-MA_{10})/SiO_2 hybrid materials. This shows peaks at 3400 and 1539 cm^{-1} which correspond to NH stretching and bending peaks of APTES. In the ratio ($NIPAM_{80}$-*co*-MA_{20})/SiO_2 a new peak is obtained in the region 1695 cm^{-1} corresponds to the acid C=O peak. As the amount of APTES is increased at par with the maleic anhydride ratio, the intensity of the peaks in the region 1695 cm^{-1} was gradually increased due to the formation of maleamic acid from the partial hydrolysis of maleic anhydride. The broadening at the region 2963-2850 cm^{-1} depicted the isopropyl groups due to the use of an increased amount of APTES. The intensity of Si-O-Si stretching and bending in the region 1080 and 957 cm^{-1} were observed. The FTIR spectra confirmed the incorporation of more amount of silica in hybrid material with monomeric ratio 60:40 ($NIPAM_{60}$-*co*-MA_{40}). After washing with THF, the peak intensity remains the same showing a strong chemical interaction between organic-inorganic hybrid frameworks.

SEM micrograph of hybrid material (Fig. 2) revealed that NIPAM-*co*-MA/SiO_2 has a well porous network-like structure

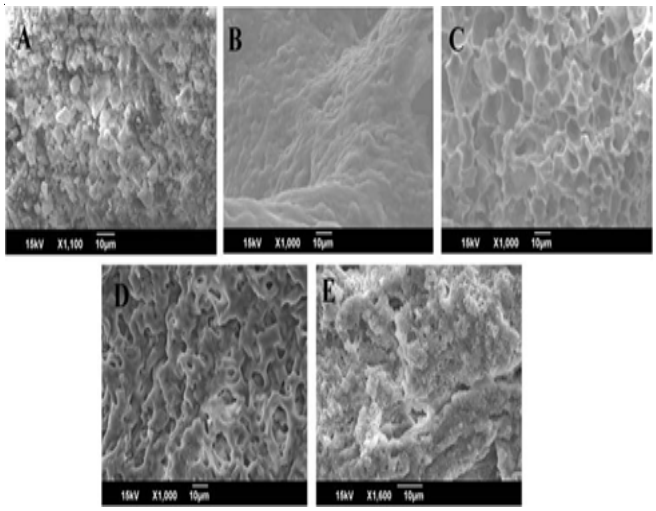

Fig. 2. SEM images of (A) $NIPAM_{80}$-*co*-MA_{20} and hybrid material with different ratios (B) ($NIPAM_{90}$-*co*-MA_{10})/SiO_2 (C) ($NIPAM_{80}$-*co*-MA_{20})/SiO_2 (D) ($NIPAM_{70}$-*co*-MA_{30})/SiO_2 (E) ($NIPAM_{60}$-*co*-MA_{40})/SiO_2

unlike in the case of neat copolymer (Fig. 2A). The particles were aggregated to make a crosslinked network like structures in the ratio (90:10). When the polymer feed ratio is decreased up to 60:40, the particles were separated and porous structure is distinctly mentioned.

TEM images (Fig. 3) of the hybrid material revealed that the particle size of hybrid material with 10 % MA have a smaller size, and increased gradually dependent upon the higher content of the MA units. Fig. 3(A) shows that the polymer ratio is more prominent than silica, and thereby the polymer is encapsulated with silica, like a core-shell structure. In the ratio 80:20 (Fig. 3B), silica content is somewhat increased, hence the silica is more apparent in the hybrid material. NIPAM-*co*-MA forms a spherical structure and the silica is interconnected network structure. In the ratio 70:30 (Fig. 3C), an internal core is formed and also more silica is incorporated which is prominent in the TEM image. The ratio 60:40 (Fig. 3D) shows that the total size was increased depending upon the more silica content. The dark sphere like regions show the silica part and the light portions show the polymer. The particle size of the hybrid material is approximately 200 nm.

The topography and phase mode of hybrid material with different ratios are presented in Fig. 4. It was observed that the silica particles were distributed homogeneously and interconnected with the polymer matrix and this is the clear evidence for the network. In the 90:10 ratio, aggregation is higher. It is not just due to the silica particles but because of the hydrophobic PNIPAM also. This increases the height (Z-axis value) of the image. But in case of 60:40 ratio, hydrophilicity reduces by the incorporation of more silica units, and we get the hydrophobic thin film. The roughness of the film is very high compared to 90:10 because of the high silica content present in the system. The particles were heterogeneous in size but homogeneously distributed in the film.

XRD pattern of pure silica, PNIPAM and hybrid materials with different ratios are shown in Fig. 5. For PNIPAM without silica, two wide peaks were observed at around $2\theta = 7.5^{\circ}$ and 19.9° respectively, which is in good agreement with the XRD pattern of the semi-crystalline pure PNIPAM. The XRD pattern

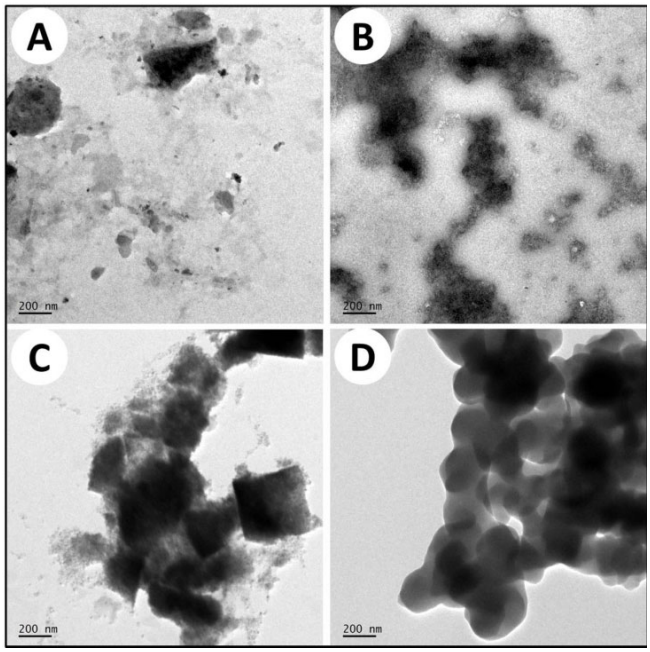

Fig. 3. Transmission Electron Micrographs of hybrid materials with different ratios (A) (NIPAM$_{90}$-*co*-MA$_{10}$)/SiO$_2$ (B) (NIPAM$_{80}$-*co*-MA$_{20}$)/SiO$_2$ (C) (NIPAM$_{70}$-*co*-MA$_{30}$)/SiO$_2$ (D) (NIPAM$_{60}$-*co*-MA$_{40}$)/SiO$_2$

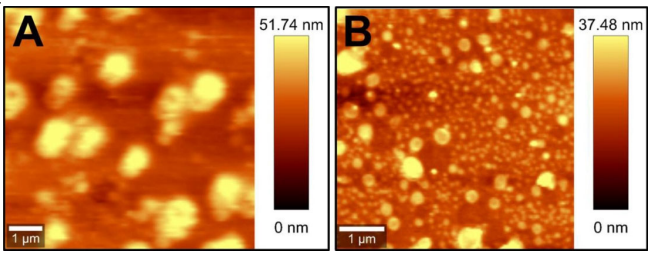

Fig. 4. AFM images of hybrid materials with different ratios (A) (NIPAM$_{90}$-*co*-MA$_{10}$)/SiO$_2$ (B) (NIPAM$_{60}$-*co*-MA$_{40}$)/SiO$_2$

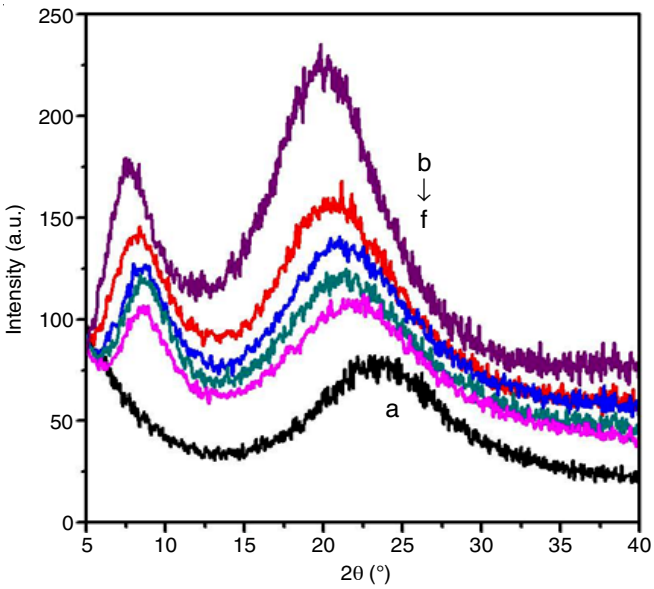

Fig. 5. XRD patterns of PNIPAM, SiO$_2$ and (NIPAM-*co*-MA)/SiO$_2$ hybrid materials, (a) pure silica, (b) PNIPAM, (c) (NIPAM$_{90}$-*co*-MA$_{10}$)/SiO$_2$ (d) (NIPAM$_{80}$-*co*-MA$_{20}$)/SiO$_2$ (e) (NIPAM$_{70}$-*co*-MA$_{30}$)/SiO$_2$ (f) (NIPAM$_{60}$-*co*-MA$_{40}$)/SiO$_2$

of pure SiO$_2$ shows only a broad peak around 2θ = 23.5° which confirm the amorphous nature of SiO$_2$ [27]. When SiO$_2$ was incorporated in PNIPAM, the position and intensity of the peak changed. The complimentary increase and decrease of SiO$_2$ and NIPAM units, respectively result in the shift of 2θ values to the higher range. The shift of 2θ =7.5° of PNIPAM may be attributed to the change in backbone structure of polymer due to the random distribution of comonomers. But the increase of 2θ = 19.9° of PNIPAM is due to the shift towards silica structure arising from the higher content of silica.

The thermal stability of prepared hybrid materials was studied using TGA (Fig. 6). The hybrid material with 40 % silica has higher thermal stability compared to hybrid material with 10 % silica because silica has high thermal stability. The thermal stability was gradually increased due to the addition of more silica content. The first stage of decomposition is observed between 50 to 125 ºC which is due to the adsorbed water and the residual solvents [28,29]. The main decomposition occurs at 350- 430 ºC corresponds to the degradation of main polymer chain [30]. The decomposition rate was decreased due to the increased content of maleic anhydride and silica. From TGA results. the obtained hybrid material exhibits higher thermal stability with the addition of silica content.

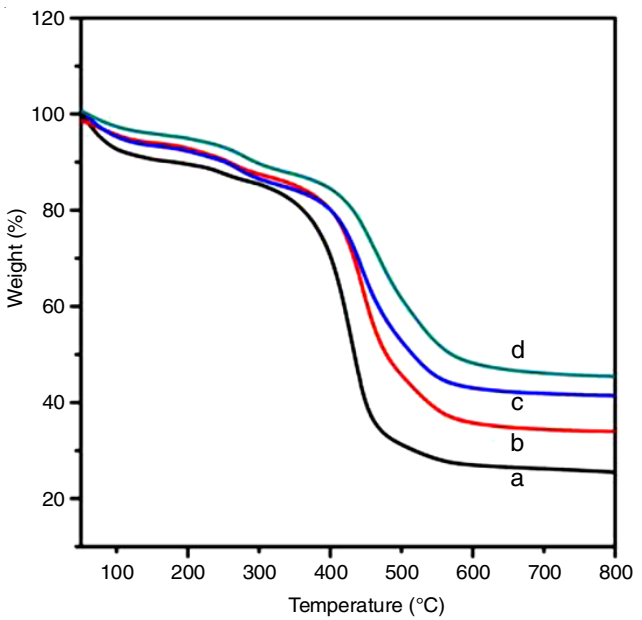

Fig. 6. TGA curves of hybrid materials with different ratios (a) (NIPAM$_{90}$-*co*-MA$_{10}$)/SiO$_2$ (b) (NIPAM$_{80}$-*co*-MA$_{20}$)/SiO$_2$ (c) (NIPAM$_{70}$-*co*-MA$_{30}$)/SiO$_2$ (d) (NIPAM$_{60}$-*co*-MA$_{40}$)/SiO$_2$

Lower critical solution temperatures (LCST) of copolymer and hybrids were measured in water at pH 7. The copolymers with ratio 90:10 and 80:20 were completely soluble in water, and showed higher LCST. The interaction of PNIPAM with water molecules is the main reason for the increase in LCST. But in case of 70:30 and 60:40, the copolymer is only partially soluble, because of the increased maleic anhydride units. The MA units interrupt the interaction of PNIPAM and water molecules.

The hybrid materials also showed similar behaviour (Table-1). Due to more NIPAM units, ratios such as 90:10 and 80:20 were completely soluble. They show higher LCST such as for 90:10 and 80:20 ratios the values were 42 and 40.5, respectively. Here in the case of 70:30 and 60:40 ratios, the solution becomes turbid because of bigger silica particles and maleamic acid units.

TABLE-1
LCST OF HYBRID MATERIALS WITH DIFFERENT RATIOS

PNIPAM-co-MA/SiO_2 monomer feed ratio (%)	LCST at pH 7
90:10	42.0
80 20	40.5
70 30	38.5
60 40	36.0

Frequency dependence on dielectric constant, dielectric loss and ac conductivity of the prepared copolymers are shown in Fig 7. The dielectric constant of the polymer was increased initially and decreased as a function of frequency due to the presence of polarizable bonds in NIPAM-*co*-MA copolymer. Fig. 8(A & B) shows the dielectric constant and dielectric loss of (NIPAM-*co*-MA)/SiO_2 hybrids measured over frequency. The dielectric constant of pure silica is less than 2.8 at 10 kHz [31]. As compared to the copolymers, the HM exhibited a higher dielectric constant (DE) which is due to the incorporation of higher polymer content. HM with ratio 60:40 ratio exhibits the lowest DE at less than 19.5 at 1 MHz. This decrease is in agreement with the increased silica content. The DE value is very much higher as compared to other hybrid material such as PI/SiO_2 and PMMA/SiO_2 which was reported earlier [32,33]. The reason for the increase of dielectric strength was due to the presence of polarizable bonds such as OH, C=O, C-N bonds contained in the (NIPAM-*co*-MA)/SiO2 hybrid material. The dielectric loss was also increased due to the blocking of charge carriers by the silica. The variations in dielectric constant at lower frequencies attained from the existence of interface polarization. It is because of the presence of impurities, surface space charge and orientation of dipoles [34,35]. In our studies, the DE value of hybrid is increased by eightfold due to the presence of polarizable groups in the polymer. So, on comparing the processability of hybrid the increase in DE value may be compromised for specific applications.

In the AC conductivity measurements, a noticeable increase in conductivity values is observed. Fig. 9A depicted AC conductivity of the hybrid materials. In the case of AC conductivity values of hybrids as the silica content increases variation at lower frequencies is changed to almost uniform values at higher frequencies. This might be due to the non-conducting nature of silica reinforcement at lower frequency values. The AC conductivity of the copolymer was found to be almost same as that of the hybrid at all the given frequencies, which showed non-conducting nature of the material in both cases (Figs. 7C and 9A). The variation of the dielectric constant as a function of silica content is shown in Fig. 9B. This means that dielectric constant increases with the higher interaction of silica content with polymer at 1 kHz frequency value.

Conclusion

(NIPAM-*co*-MA)/SiO_2 hybrid materials were easily prepared with varying compositions of both organic and inorganic componentsThey were prepared by fine-tuning the synthetic protocol for coupling N-isopropyl acrylamide, maleic anhydride and aminopropyl triethoxy silane through sol-gel technique in the absence of externally added acid or base catalyst. The chemical linking between the organic and inorganic groups were confirmed by solubility studies and IR spectroscopy.

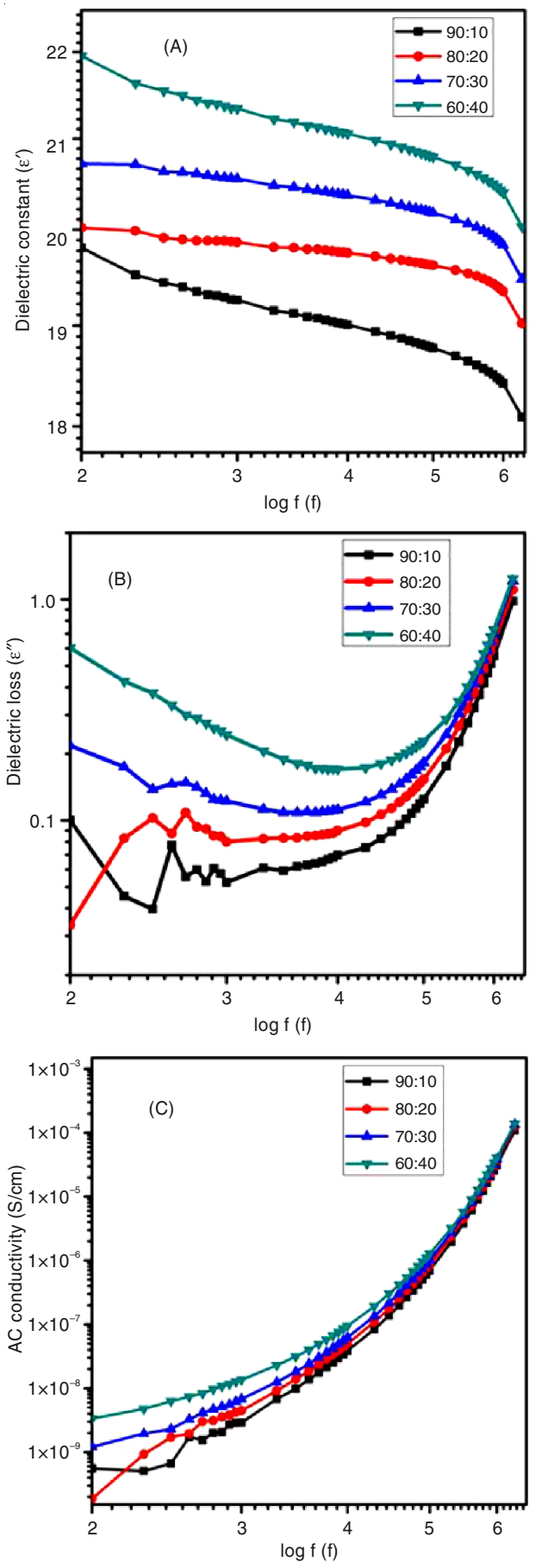

Fig. 7. Frequency dependant (A) Dielectric constant (B) Dielectric loss and (C) AC conductivity of NIPAM-*co*-MA copolymers

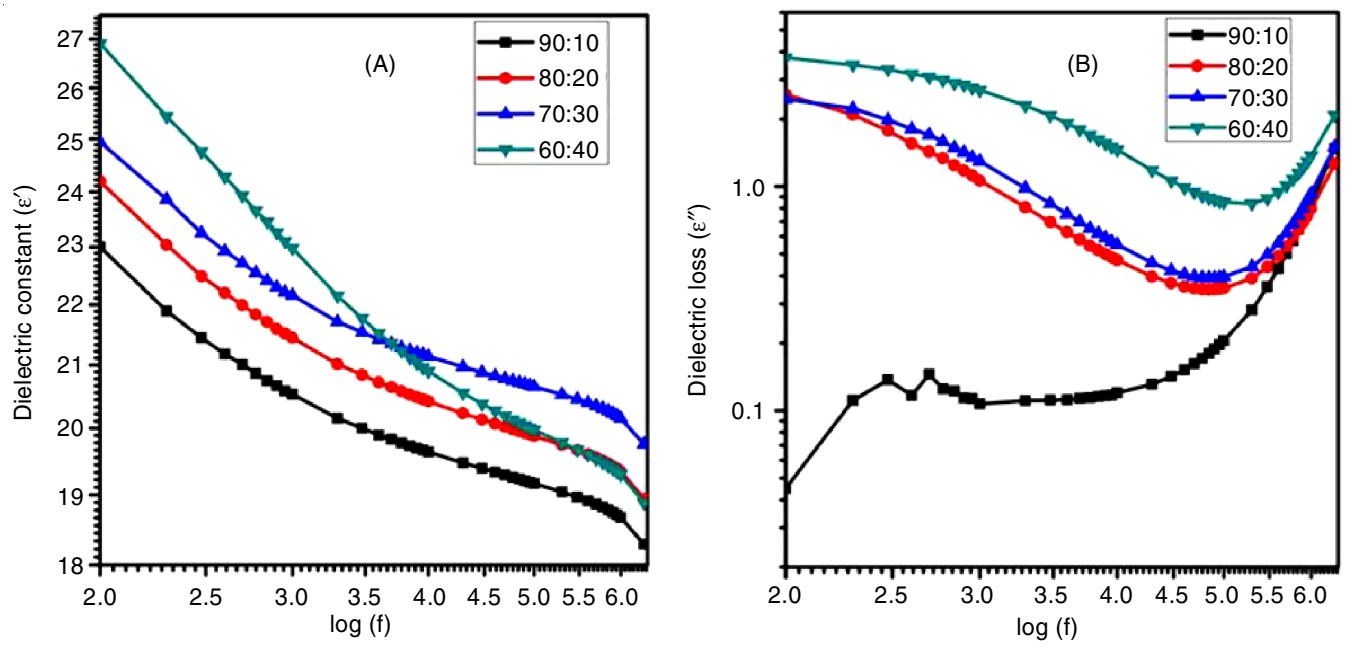

Fig. 8. Frequency dependant (A) Dielectric constant and (B) Dielectric loss of (NIPAM-*co*-MA)/SiO_2 hybrid materials

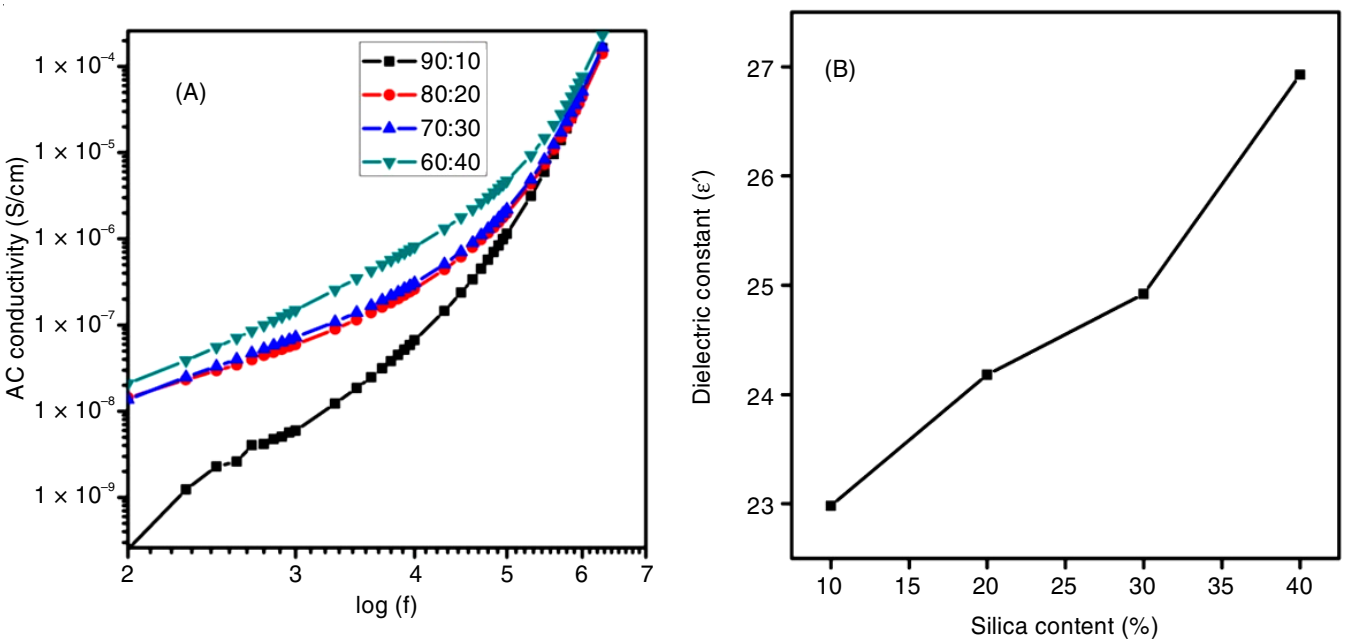

Fig. 9. Frequency dependant (A) AC conductivity and (B) Variation in dielectric constant with silica content at 1000 Hz of hybrid materials

SEM, TEM and AFM images established the existence of highly porous inorganic nanodomains. TGA and XRD did the thermal stability and crystallinity studies. Dielectric studies revealed that these materials possess slightly higher as that of other silica hybrid materials however with better process-ability compared to that of pure silica along with good thermal stability.

ACKNOWLEDGEMENTS

The authors are thankful to DST, FIST, CSIR and UGC for their generous funding. One of the authors (GPG) gratefully acknowledges Kerala State e-grantz for fellowship.

REFERENCES

1. F. Mammeri, E.L. Bourhis, L. Rozes and C. Sanchez, *J. Mater. Chem.*, **15**, 3787 (2005); https://doi.org/10.1039/b507309j.
2. M. Okamoto, *Mater. Sci. Technol.*, **22**, 756 (2006); https://doi.org/10.1179/174328406X101319.
3. D.A. Koleva, N. Boshkov, V. Bachvarov, H. Zhan, J.H.W. de Wit and K. van Breugel, *Surf. Coat. Technol.*, **204**, 3760 (2010); https://doi.org/10.1016/j.surfcoat.2010.04.043.
4. M.A. Ver Meer, B. Narasimhan, B.H. Shanks and S.K. Mallapragada, *ACS Appl. Mater. Interfaces*, **2**, 41 (2010); https://doi.org/10.1021/am900540x.
5. G.L. Li, Z. Zheng, H. Mo¨hwald and D.G. Shchukin, *ACS Nano*, **7**, 2470 (2013); https://doi.org/10.1021/nn305814q.

6. J. Chen, M. Liu, C. Chen, H. Gong and C. Gao, *Appl. Mater. Interf.*, **3**, 3215 (2011); https://doi.org/10.1021/am2007189.
7. C. Wang, J. Wang, W. Gao, J.Q. Jiao, H.J. Feng, X. Liu and L. Chen, *J. Colloid Interface Sci.*, **343**, 141 (2010); https://doi.org/10.1016/j.jcis.2009.11.005.
8. K. Zhang, J. Ma, B. Zhang, Sh. Zhao, Y.P. Li, Y.X. Xu, W. Yu and J. Wang, *Mater. Lett.*, **61**, 949 (2007); https://doi.org/10.1016/j.matlet.2006.06.021.
9. P. Liu, W. Liu and Q. Xue, *Mater. Chem. Phys.*, **87**, 109 (2004); https://doi.org/10.1016/j.matchemphys.2004.05.001.
10. M. Heskins and J.E. Guillet,, *J. Macromol. Sci. Chem.*, **A2**, 1441 (1968); https://doi.org/10.1080/10601326808051910.
11. R. Pelton, *J. Colloid Interface Sci.*, **348**, 673 (2010); https://doi.org/10.1016/j.jcis.2010.05.034.
12. J.H. Park, Y.H. Lee and S.G. Oh, *Macromol. Chem. Phys.*, **208**, 2419 (2007); https://doi.org/10.1002/macp.200700247.
13. J. Robertson, *Eur. Phys. J. Appl. Phys.*, **28**, 265 (2004); https://doi.org/10.1051/epjap:2004206.
14. F. Hoffmann, M. Cornelius, J. Morell and M. Froba, *Angew. Chem. Int. Ed.*, **45**, 3216 (2006); https://doi.org/10.1002/anie.200503075.
15. B. Luo, X. Wang, E. Tian, H. Gong, Q. Zhao, Z. Shen, Y. Xu, X. Xiao and L. Li, *ACS Appl. Mater. Interfaces*, **8**, 3340 (2016); https://doi.org/10.1021/acsami.5b11231.
16. T. Zhou, J.W. Zha, Y. Hou, D. Wang, J. Zhao and Z.M. Dang, *ACS Appl. Mater. Interfaces*, **3**, 4557 (2011); https://doi.org/10.1021/am201454e.
17. Z.Y. Zhou, S.M. Zhu and D. Zhang, *J. Mater. Chem.*, **17**, 2428 (2007); https://doi.org/10.1039/b618834f.
18. Q. Fu, G.V. Rama Rao, T.L. Ward, Y. Lu and G.P. Lopez, *Langmuir*, **23**, 170 (2007); https://doi.org/10.1021/la062770f.
19. K. Manivannan, C.C. Cheng and J.K. Chen, *Electroanalysis*, **29**, 1443 (2017); https://doi.org/10.1002/elan.201600755.
20. H. Byun, J. Hu, P. Pakawanit, L. Srisombat and J.-H. Kim, *Nanotechnology*, **28**, 025601 (2017); https://doi.org/10.1088/0957-4484/28/2/025601.
21. Y.-G. Lee, C.-Y. Park, K.-H. Song, S.-S. Kim and S.-G. Oh, *J. Ind. Eng. Chem.*, **18**, 744 (2012) https://doi.org/10.1016/j.jiec.2011.11.117.
22. Y.Z. You, K.K. Kalebaila, S.L. Brock and D. Oupicky, *Chem. Mater.*, **20**, 3354 (2008); https://doi.org/10.1021/cm703363w.
23. S.A. Jadhav, I. Miletto, V. Brunella, G. Berlier and D. Scalarone, *Polym. Adv. Technol.*, **26**, 1070 (2015); https://doi.org/10.1002/pat.3534.
24. H. Kesim, Z.M.O. Rzaev, S. Dincer and E. Piskin, *Polymer*, **44**, 2897 (2003); https://doi.org/10.1016/S0032-3861(03)00177-0.
25. R. Francis, C.P. Jijil, C.A. Prabhu and C.H. Suresh, *Polymer*, **48**, 6707 (2007); https://doi.org/10.1016/j.polymer.2007.08.061.
26. W. Zhou, J. Hua, D. Kun, Y. Qiu and Y. Wei, *J. Polym. Sci.: Polym. Chem.*, **36**, 1607 (1998); https://doi.org/10.1002/(SICI)1099-0518(19980730)36:10<1607::AID-POLA13>3.0.CO;2-K.
27. B.-S. Tian and C. Yang, *J. Phys. Chem. C*, **113**, 4925 (2009); https://doi.org/10.1021/jp808534q.
28. J. Wang, X. Lu, N. Huang, H. Zhang, R. Li and W. Li, *Mater. Sci. Eng. B*, **224**, 1 (2017); https://doi.org/10.1016/j.mseb.2017.07.003.
29. P. Banet, P. Griesmar, S. Serfaty, F. Vidal, V. Jaouen and J.-Y. Le Huerou, *J. Phys. Chem. B*, **113**, 14914 (2009); https://doi.org/10.1021/jp906229n.
30. A. Alli and B. Hazer, *Eur. Polym. J.*, **44**, 1701 (2008); https://doi.org/10.1016/j.eurpolymj.2008.04.004.
31. J.J. Park, *Trans. Electr. Electron. Mater.*, **13**, 322 (2012); https://doi.org/10.4313/TEEM.2012.13.6.322.
32. S. Babanzadeh, S. Mehdipour-Ataei and A.R. Mahjoub, *Des. Monomers Polym.*, **16**, 417 (2013); https://doi.org/10.1080/15685551.2012.747159.
33. M.D. Morales-Acosta, M.A. Quevedo-Lopez, B.E. Gnade and R. Ramirez-Bon, *J. Sol-Gel Sci. Technol.*, **58**, 218 (2011); https://doi.org/10.1007/s10971-010-2380-9.
34. G. Hou, B. Cheng, F. Ding, M. Yao, Y. Cao, P. Hu, R. Ma and F. Yuan, *RSC Adv.*, **5**, 9432 (2015); https://doi.org/10.1039/C4RA14212H.
35. M. Shahbazi, A. Bahari and S. Ghasemi, *Org. Electron.*, **32**, 100 (2016); https://doi.org/10.1016/j.orgel.2016.02.012.